nature geoscience

LETTERS

PUBLISHED ONLINE: 22 MAY 2011 | DOI: 10.1038/NGEO1156

Seasonal and spatial variations of Southern Ocean diapycnal mixing from Argo profiling floats

Lixin Wu[1]*, Zhao Jing[1], Steve Riser[2] and Martin Visbeck[3]

The Southern Ocean is thought to be one of the most energetic regions in the world's oceans. As a result, it is a location of vigorous diapycnal mixing of heat, salt and biogeochemical properties[1–3]. At the same time, the Southern Ocean is poorly sampled, not least because of its harsh climate and remote location. Yet the spatial and temporal variation of diapycnal diffusivity in this region plays an important part in the large-scale ocean circulation and climate[4–6]. Here we use high-resolution hydrographic profiles from Argo floats in combination with the Iridium communications system to investigate diapycnal mixing in the Southern Ocean. We find that the spatial distribution of turbulent diapycnal mixing in the Southern Ocean at depths between 300 and 1,800 m is controlled by the topography, by means of its interaction with the Antarctic Circumpolar Current. The seasonal variation of this mixing can largely be attributed to the seasonal cycle of surface wind stress and is more pronounced in the upper ocean over flat topography. We suggest that additional high-resolution profiles from Argo floats will serve to advance our understanding of mixing processes in the global ocean interior.

The Southern Ocean is an important source of bottom water in the world's oceans and is a key upwelling site of deep water, pointing to diapycnal mixing (that is, mixing across surfaces of equal density) in the region as an important controlling factor of the global meridional overturning circulation (MOC; refs 7,8). Modelling studies have demonstrated that the global strength of the MOC depends critically on the details of the representation of mixing processes in the Southern Ocean interior[9]. A few existing observations[10–14] in this region have revealed dramatic spatial heterogeneity in diapycnal mixing, with values of diffusivity over smooth topography comparable to those in the mid-latitude ocean interior (of the order of $10^{-5}\,m^2\,s^{-1}$), and enhanced mixing (of the order of $10^{-4}\,m^2\,s^{-1}$ or larger) extending far from rough topography. However, discerning the nature of diapycnal mixing over the entire Southern Ocean is still a formidable challenge because of the very limited sampling of the necessary parameters in the region. Furthermore, in general the temporal variability of diapycnal mixing remains poorly assessed and understood throughout most of the world's oceans, but in some cases the causes of such variability might be reasonably straightforward to document. As an example, recent analysis of historical hydrographic data reveals that the subsurface turbulent diapycnal mixing in the Northwestern Pacific displays a pronounced seasonal variability stirred by surface wind stress[15].

The International Argo Program has created the first global array for observing the subsurface ocean. A subset of Argo floats deployed are designed to use the Iridium communications system (henceforth referred to as Argo Iridium floats), and are able to provide high-resolution (2 m) profiles that are able to resolve fine-scale (tens to hundreds of meters) strain. These floats provide an unprecedented opportunity to determine the geographic distribution of upper ocean turbulent diapycnal mixing worldwide, especially in locations with unfavourable weather and logistical limitations. Furthermore, these long-term floats with high temporal coverage also have the potential ability to access the temporal variations of diapycnal mixing over a vast region. Here we will make the first attempt to demonstrate the ability of these high-resolution profiles from Argo Iridium floats to map both the seasonal and spatial distribution of diapycnal mixing in the upper Southern Ocean by employing a fine-scale parameterization method[12,16](see Methods for details), which displays the capability to estimate diapycnal mixing in the upper ocean[15,17,18].

The Southern Ocean contains a wide range of topographic features (Fig. 1a). Although Argo Iridium floats do not cover the entire Southern Ocean, the water column over the roughest topography (except the Pacific Antarctic Ridge) has been well sampled, making it possible to capture most hotspots of turbulent diapycnal mixing in the Southern Ocean (Fig. 1a). The diapycnal diffusivity derived from Argo Iridium floats shows significant spatial variability (Fig. 1b). Whereas low and moderate mixing rates (on the order of $10^{-5}\,m^2\,s^{-1}$) are found over the abyssal plains in the southeast Pacific and to the south of Australia, enhanced mixing (on the order of $10^{-4}\,m^2\,s^{-1}$ or larger) is found over rough topography, including the Scotia Sea, the Drake Passage, east of the Kerguelen Plateau, the Mid-Atlantic and Southwest Indian ridges, and the edges of the Campbell Plateau and Antarctica (Fig. 1b). This enhanced mixing along topographic features can be further inferred from the vertical map of the diapycnal diffusivity and dissipation rate (Fig. 2a–c), where most of the enhanced mixing corresponds to the large roughness values (variance of bottom height). This is also demonstrated by the significant correlation between the values of diapycnal diffusivity and bottom roughness (Fig. 3a). A notable exception occurs in the region 50°–70° E, where the dissipation rate is much stronger in the depth range from 300 to 900 m, even though the topography is relatively smooth. The enhanced mixing here is possibly owing to the great amount of work done by the wind on inertial motions[19] in the region.

The origin of the mixing may be inferred from the energy budget. Over relatively smooth topography, the turbulent kinetic dissipation rate decreases with depth throughout the sampled water column (300–1,800 m; Fig. 3b), and the vertically integrated dissipation rate is about $1.8 \times 10^{-3}\,W\,m^{-2}$, comparable in magnitude to regional estimates of the energy flux from the wind to near-inertial motions[19]. On the other hand, over rough topography, the dissipation rate in the upper 300–1,200 m also decreases with depth, and deviates from that over smooth topography by a factor of only two. However, below 1,200 m, over rough topography the depth trend of dissipation rate is reversed and the deviation is a factor of more than five (Fig. 3b). These enhanced dissipation rates are probably owing to the breaking of internal

[1]Physical Oceanography Laboratory, Ocean University of China, Qingdao 266003, China, [2]School of Oceanography, University of Washington, Seattle, Washington 98195, USA, [3]IFM-GEOMAR, Gebäude Westufer, Düsternbrooker Weg 20, 24105 Kiel, Germany. *e-mail: lxwu@ouc.edu.cn.

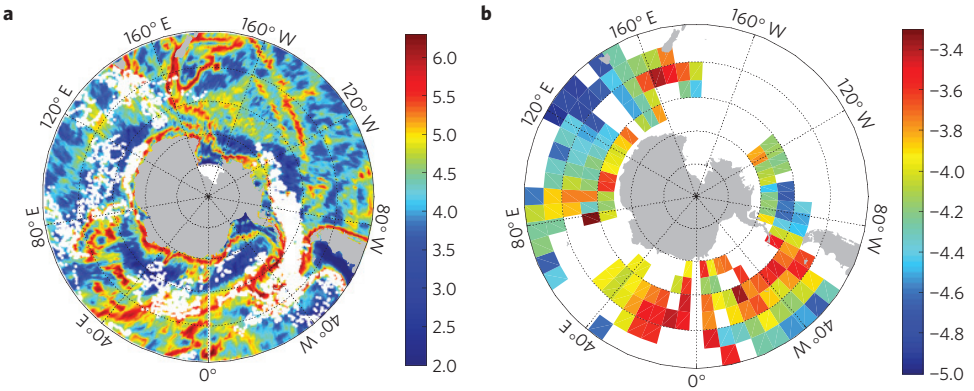

Figure 1 | Horizontal distribution of topographic roughness and diapycnal diffusivity in the Southern Ocean. a, Topographic roughness and geographic distribution of high-resolution profiles (white dots) obtained from the Argo Iridium floats used in the Southern Ocean and described in this paper. The colour scale represents Log_{10}(Roughness) in m^2. **b**, Horizontal distribution of diapycnal diffusivity, vertically averaged over the depth range 300–1,800 m, on a 6° × 5° spatial grid. The colour scale represents $\mathrm{Log}_{10}(K)$ in $m^2\ s^{-1}$.

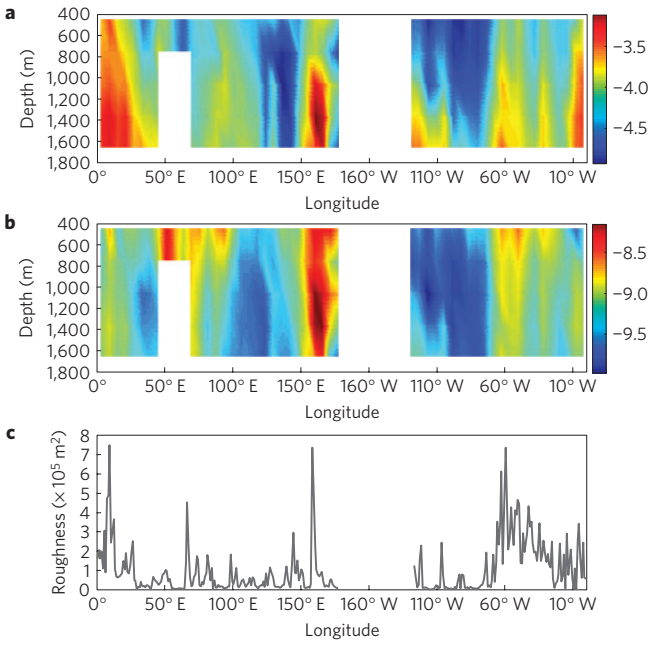

Figure 2 | Depth–longitude distribution of diffusivity, dissipation rate and roughness averaged between 40 and 75° S. a, For the time averaged diapycnal diffusivity, with colour scale representing $\mathrm{Log}_{10}(K)$ in $m^2\ s^{-1}$. **b**, For the time averaged dissipation rate, with the colour scale representing $\mathrm{Log}_{10}(\varepsilon)$ in $m^2\ s^{-3}$. **c**, For the bottom roughness (m^2).

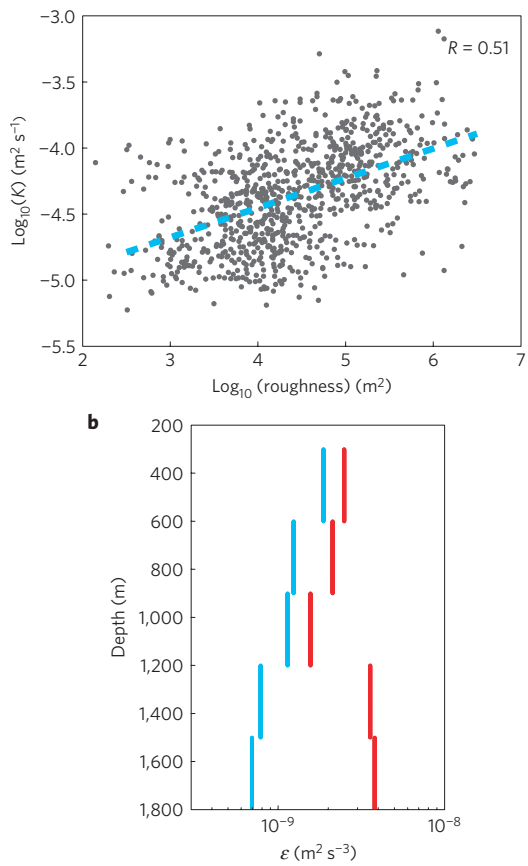

Figure 3 | Relation of diapycnal mixing to bottom roughness. a, Vertically integrated diffusivity ($m^2\ s^{-1}$) from 300 to 1,800 m plotted against bottom roughness (m^2). The linear fit (blue dashed line) as a slope of 0.22 with a 95% confidence interval between 0.19 and 0.25. **b**, Vertical profiles of dissipation rate ($m^2\ s^{-3}$) against depth over rough (red) and smooth (blue) topographies.

waves as the abyssal flow impinges on rough topography[6,10,20]. However, unlike the observations at other places[4], they extend far above topography, dominating mixing below 1,200-m depth and making a non-negligible contribution to mixing in the upper 300–1,200 m. As the velocity of bottom geostrophic flows is much larger than that of barotropic tidal flows in large parts of the Southern Ocean, the enhanced mixing is probably sustained by geostrophic motions impinging on rough topography rather than by barotropic tidal motions[10,21]. This can be estimated as follows. Assuming that the averaged dissipation rate in the deeper region is no less than that in the upper 2,000 m (not unreasonable for an energy source located at the bottom boundary[10,21]), the vertically integrated dissipation rate for a water column with a thickness of 4,000 m is at least $11.3 \times 10^{-3}\ W\ m^{-2}$, which is comparable to the rate of the work done by the wind on the Antarctic Circumpolar Current (ACC; ref. 22), further suggesting that the origin of the mixing lies with the strong larger-scale geostrophic motions.

Temporal variability of the mixing can also be expected as a result of the varying energy input from tides and wind[6,19]. Though studies have found the spring-neap cycle of the tide can modulate the turbulent dissipation significantly[23], the seasonality of the mixing still remains poorly assessed because of limited data. The high

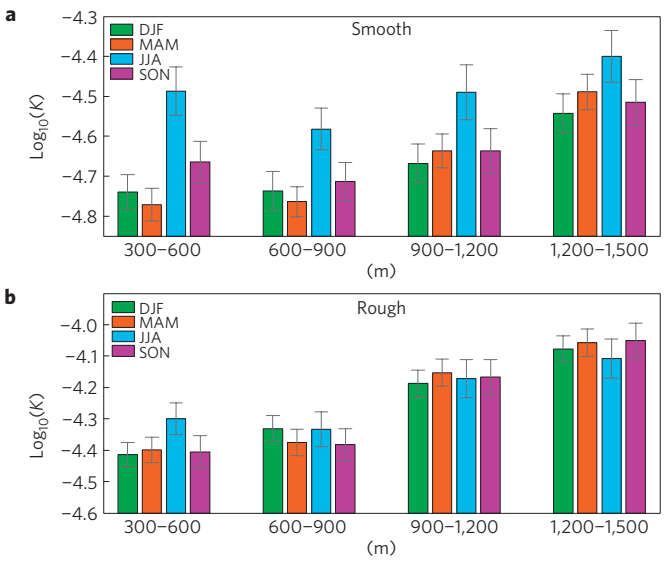

Figure 4 | Seasonal changes of diapycnal diffusivity at different depths over different topography. a, Over smooth and **b**, over rough topography. The error bars represent the 95%-confidence interval based on a log-normal distribution, which is justified by a Lilliefors test. The diffusivity evaluated here is normalized by the latitude-dependence function $j(f/N)$ (see definition in Methods section) to avoid profiles in some seasons being more weighted to high latitudes. DJF (December, January, February), MAM (March, April, May), JJA (June, July, August), SON (September, October, November).

temporal coverage of long-term Argo Iridium floats provides an opportunity for the first time to estimate the seasonal variation of turbulent diapycnal diffusivity in the whole Southern Ocean. Considering the different possible mechanisms dominating the diapycnal mixing, we have divided the profiles into two groups, over rough and over smooth topography, and profiles under severe ice-covered conditions are discarded. Over the relatively smooth topography, where the work done by the wind on inertial motions dominates the upper ocean mixing, the diapycnal diffusivity displays a distinct seasonal variation (Fig. 4a), with a maximum in winter. Such a variation probably results from the varying energy input from wind to the inertial motion. Here we computed the work done by the wind on near-inertial motions following the method of Alford[19]. Not surprisingly, the energy flux in the corresponding regions is much larger in winter (5.4×10^{-3} W m^{-2}) than in summer (2.9×10^{-3} W m^{-2}). On the other hand, although the seasonality of diapycnal mixing persists in the deep ocean, the amplitude decreases rapidly with depth. Therefore, despite a large wind-input energy, only a small portion might be able to propagate to mid-depths (1,500 m), which may account for the slightly elevated shear spectrum compared with the Garrett–Munk spectrum found at the same depth from tracer release experiments[14]in the Pacific Sector just upstream of the Drake Passage. In contrast, for the profiles over rough topography, the seasonal variation of the turbulent diapycnal mixing is less marked (Fig. 4b). This is probably because the strength of the ACC, one of the main factors dominating the diapycnal mixing here, displays no significant seasonal cycle[24].

One of the main energy sources for the upper ocean mixing is the work done by the wind on near-inertial motions[6,19]. It has been debated[6] whether a substantial fraction of this energy flux can penetrate to deep isopycnals and thus contribute to abyssal mixing. So far, neither modelling and observational studies have reached consensus[25,26]. Our results indicate that in the Southern Ocean the seasonality of diapycnal mixing controlled by the seasonal cycle of near-inertial energy flux input by wind stress extends at least to 1,500 m, pointing to the important roles of wind-input energy in maintaining the subsurface ocean mixing. This is consistent with the numerical simulation of Danioux *et al.*[25], but contradicts that of Zhai and co-workers[26]. Large amounts of downward-propagating near-inertial energy here may be the result of both enhanced eddy variability and strong near-inertial energy input from the wind in the Southern Ocean[27,28].

There are inevitable uncertainties inherent in fine-scale parameterizations[29]. Also, using strain with the value of R_ω fixed at 7 may lead to further uncertainties owing to a wide range of change in shear/strain ratio in the ocean interior. Therefore, it is necessary to compare our results with others to make a robust estimate. The tracer release experiments in the Pacific Sector just upstream of the Drake Passage revealed that the diapycnal diffusivity is $(1.3\pm0.2)\times10^{-5}$ m^2 s^{-1} near 1,500-m depth[14]. The value based on Argo Iridium float data at the same location and the same depth is about 2.5×10^{-5} m^2 s^{-1}. Furthermore, results based on LADCP/CTD data show enhanced mixing (of the order of 10^{-4} m^2 s^{-1}) in the upper ocean over the Kerguelen Plateau[12], the Drake Passage and the Scotia sea[10]. Diffusivity derived from Argo Iridium floats in the corresponding regions is of the same order, although all these estimates are based on fine-scale parameterization methods.

Although the maximum sampling depth of Argo floats is 2,000 m, the dense spatial-temporal coverage of Argo Iridium profiles greatly improve our understanding of diapycnal mixing processes in the Southern Ocean. Using ship-based ACDP/CTD profiles in the Scotia Sea, Naveira Garabato *et al.* argued that the enhanced mixing is probably caused by the geostrophic flow impinging on rough topography[10]. The much stronger mixing in the upper ocean over the rough topography throughout the Southern Ocean observed here indicates that much of the ACC path is seeded with hotspots of diapycnal mixing resulting from the interaction of geostrophic flow with bottom topography.

This work demonstrates the potential ability of Argo Iridium floats to map both the geographic distribution and temporal variations of upper ocean turbulent diapycnal mixing in global oceans, especially in locations with unfavourable weather and logistical limitations, although the absolute value of mixing inferred from Argo profiling data based on fine-scale parameterizations remains to be verified. This work also represents the first attempt to use high-resolution profiles from Argo Iridium floats to examine the seasonality of diapycnal mixing in the Southern Ocean, and reveals the distinct seasonal variations in the upper ocean controlled by the near-inertial energy input from wind stress. With increasing numbers of high-quality and high-resolution profiles becoming available, our understanding of the mixing processes in the global ocean interior will be improved greatly in the near future and should serve to improve the representation of these processes in models of the large-scale ocean circulation.

Methods

Data. The high-resolution profiles obtained from Argo floats using the Iridium communications system extend from year 2005 to 2010, with a maximum sampling depth of 2000 m. Only the profiles located within the latitude band 40°–75° S and with maximal sampling depth exceeding 1,000 m are used here, resulting in 5,337 profiles in total. All the profiles have been subjected to real-time data quality checks applied by Argo national data centres. We have broken the profiles into 300-m segments to evaluate the segment-averaged diffusivity. The shallowest segment, 0–300 m, is discarded because of the presence of sharp pycnoclines[12]. The ETOPO2v2 (2-minute Gridded Global Relief Data) is also used to evaluate the roughness. Finally, the 6-h wind stress data from NCEP/NCAR is used to compute the work done by the wind on near-inertial motions, following the method of Alford[19].

Fine-scale parameterization method. The diapycnal diffusivity can be expressed in terms of fine-scale strain as[12,16]

$$\kappa = K_0 \frac{\langle \xi_z^2 \rangle^2}{\mathrm{GM}\langle \xi_z^2 \rangle^2} h_2(R_\omega) j(f/N)$$

where ${}_{GM}\langle\xi_z^2\rangle$ is the strain variance from the Garrett–Munk model spectrum treated in the same way as the observed strain variance $\langle\xi_z^2\rangle$, and R_ω represents the shear/strain variance ratio. The latitude-dependence function $j(f/N)$ is a function of the Coriolis force (f) and the Brunt–Vaisala frequency (N) (refs 12,16)

Internal wave strain is estimated from buoyancy frequency[29]. Fourier transformation then gives the spectral representation $\phi(k)$. The strain variance $\langle\xi_z^2\rangle$ is determined by integrating $\phi(k)$ from a minimum vertical wavenumber k_{min} out to a maximum vertical wavenumber k_{max}, so that[12]

$$\langle\xi_z^2\rangle = \int_{k_{min}}^{k_{max}} \phi(k)\mathrm{d}k = 0.1$$

The constant 0.1 in the above equation is somewhat arbitrary. However, it is found that changing this constant has a only minor effect on mixing amplitudes and does not affect our conclusions here. The GM strain variance is computed over the same wavenumber band.

The dissipation rate can be expressed in the form

$$\varepsilon = K\frac{N^2}{\Gamma}$$

where Γ is mixing efficiency, typically taken to be 0.2 (ref. 30).

The strain spectrum may be contaminated as a result of strong depth changes in the background stratification[12]. Great depth variability in the background stratification under 300-m depth is found in some profile segments here and contamination at the lowest resolved wavenumbers leaks to higher wavenumbers, which may result in a serious overestimation. Here we develop a simple test inspired by Kunze *et al.*[12] to exclude these seemingly 'bad' profile segments. For each 300-m segment, we evaluate a linear fit to the potential density profiles. By inspecting the numbers of profile segments with lower strain variance, we find that the excessive redness of the lower-variance strain spectra is generally confined to the lowest resolved wave numbers, as is the contamination by background stratification when the regression coefficient is larger than 0.98. Thus, segments with regression coefficients less than 0.98 have been discarded to eliminate the contamination by background stratification. In fact, the results in this paper, which are statistically based on large numbers of profiles, are not sensitive to the choice of the critical value, and changing this value from 0.95 to 0.99 leads to no substantial differences in our results.

On the other hand, the strain spectra can also be contaminated by instrument noise[12]. The noise level is spectrally determined here. Assuming that the instrument noise roughly satisfies a white noise model, we found that even in the deepest segment (1,500–1,800 m), over smooth topography, the bias in the estimated diffusivity is less than 60% owing to the contamination by noise, much less than the uncertainties resulting from the fine-scale parameterization itself (a factor of 3–4). As the strain spectrum is more unlikely to be affected by noise in the shallower segments over rough topography, where background stratification is stronger and strain variance is higher, it gives us confidence that the strain variance computed from the hydrographic profiles of the Argo Iridium floats is reliable.

As profiles of horizontal velocity are not available, it is difficult to estimate R_ω. Here R_ω is set to 7, based on the results estimated by Kunze and co-workers[12]. As the fine-scale parameterization was only able to reproduce microstructure diffusivities within a factor of 2 (ref. 29), using strain with only a fixed value of R_ω might lead to uncertainties in diapycnal diffusivity of a factor of 3–4.

The bottom roughness here represents the variance of bottom height H in m^2 and is computed over a 1° (longitude) × 0.5° (latitude) box, which is approximately a 50 km × 50 km domain. Following that, the bottom roughness is gridded onto a 1° × 1° spatial grid. Here smooth topography is defined as regions with a value of roughness less than 2×10^4 m^2 and the rough topography as that with values larger than 2×10^4 m^2. The critical value is chosen by visually inspecting Fig. 1a and is thus to some extent arbitrary. However, changing this value does not result in any substantial differences to the results here.

Received 20 December 2010; accepted 15 April 2011; published online 22 May 2011

References

1. Sarmiento, J. L. & Toggweiler, J. R. A new model for the role of the oceans in determining atmospheric pCO_2. *Nature* **308,** 621–624 (1984).
2. Heywood, K. J., Naveira Garabato, A. C. & Stevens, D. P. High mixing rates in the abyssal Southern ocean. *Nature* **415,** 1011–1014 (2002).
3. Gregory, J. M. Vertical heat transports in the ocean and their effect on time dependent climate change. *Clim. Dyn.* **16,** 501–515 (2000).
4. Polzin, K., Toole, J., Ledwell, J. & Schmitt, R. Spatial variability of turbulent mixing in the abyssal ocean. *Science* **276,** 93–96 (1997).
5. Saenko, O. & Merryfield, W. On the effect of topographically enhanced mixing on the global ocean circulation. *J. Phys. Oceanogr.* **35,** 826–834 (2005).
6. Wunsch, C. & Ferrari, R. Vertical mixing, energy and the general circulation of the oceans. *Annu. Rev. Fluid Mech.* **36,** 281–412 (2004).
7. Huang, R. X. Mixing and energetics of the oceanic thermohaline circulation. *J. Phys. Oceanogr.* **29,** 727–746 (1999).
8. Zhang, J., Schmitt, R. W. & Huang, R. X. The relative influence of diapycnal mixing and hydrologic forcing on the stability of the thermohaline circulation. *J. Phys. Oceanogr.* **29,** 1096–1108 (1999).
9. Jayne, S. R. The Impact of abyssal mixing parameterizations in an Ocean General Circulation Model. *J. Phys. Oceanogr.* **39,** 1756–1775 (2009).
10. Naveira Garabato, A. C., Polzin, K. L., King, B. A., Heywood, K. J. & Visbeck, M. Widespread intense turbulent mixing in the Southern Ocean. *Science* **303,** 210–213 (2004).
11. Sloyan, B. M. Spatial variability of mixing in the southern ocean. *Geophys. Res. Lett.* **32,** L18603 (2005).
12. Kunze, E., Firing, E., Hummon, J. M., Chereskin, T. K. & Thurnherr, A. M. Global abyssal mixing inferred from lowered ADCP shear and CTD strain profiles. *J. Phys. Oceanogr.* **36,** 1553–1576 (2006).
13. Polzin, K. L. & Firing, E. *International WOCE Newsletter, No. 29*, WOCE International Project Office, Southampton, United Kingdom, 39–42 (1997).
14. Ledwell, J. R., St Laurent, L. C., Girton, J. B. & Toole, J. M. Diapycnal mixing in the Antarctic Circumpolar Current. *J. Phys. Oceanogr.* **41,** 241–246 (2011).
15. Jing, Z. & Wu, L. Seasonal variation of turbulent diapycnal mixing in the northwestern Pacific stirred by wind stress. *Geophys. Res. Lett.* **37,** L23604 (2010).
16. Gregg, M. C., Sanford, T. B. & Winkel, D. P. Reduced mixing from the breaking of internal waves in equatorial ocean waters. *Nature* **422,** 513–515 (2003).
17. Finnigan, T., Luther, D. & Lukas, R. Observations of enhanced diapycnal mixing near the Hawaiian Ridge. *J. Phys. Oceanogr.* **32,** 2988–3002 (2002).
18. Thompson, A. F., Gille, S. T., MacKinnon, J. A. & Sprintall, J. Spatial and temporal patterns of small-scale mixing in Drake Passage. *J. Phys. Oceanogr.* **37,** 572–592 (2007).
19. Alford, M. H. Improved global maps and 54-year history of wind work on ocean inertial motions. *Geophys. Res. Lett* **30,** 1424 (2003).
20. Bell, T. H. Topographically generated internal waves in the open ocean. *J. Geophys. Res.* **80,** 320–327 (1975).
21. Nikurashin, M. & Ferrari, R. Radiation and dissipation of internal waves generated by geostrophic motions impinging on small-scale topography: Application to the Southern Ocean. *J. Phys. Oceanogr.* **40,** 2025–2042 (2010).
22. Wunsch, C. The work done by the wind on the oceanic general circulation. *J. Phys. Oceanogr.* **28,** 2332–2340 (1998).
23. Klymak, J. M., Pinkel, R. & Rainville, L. Direct breaking of the internal tide near topography: Kaena Ridge, Hawaii. *J. Phys. Oceanogr.* **38,** 380–399 (2008).
24. Sprintall, J. Seasonal to interannual upper-ocean variability in the Drake Passage. *J. Mar. Res.* **61,** 27–57 (2003).
25. Danioux, E., Klein, P. & Rivière, P. Propagation of wind energy into the deep ocean through a fully turbulent mesoscale Eddy field. *J. Phys. Oceanogr.* **38,** 2224–2241 (2008).
26. Zhai, X., Greatbatch, R. J., Eden, C. & Hibiya, T. On the loss of wind-induced near-inertial energy to turbulent mixing in the upper ocean. *J. Phys. Oceanogr.* **39,** 3040–3045 (2009).
27. Zhai, X., Greatbatch, R. J. & Zhao, J. Enhanced vertical propagation of storm-induced near-inertial energy in an eddying ocean channel model. *Geophys. Res. Lett.* **32,** L18602 (2005).
28. Kunze, E. Near-inertial propagation in geostrophic shear. *J. Phys. Oceanogr.* **15,** 544–565 (1985).
29. Polzin, K. L., Toole, J. M. & Schmitt, R. W. Finescale parameterizations of turbulent mixing. *J. Phys. Oceanogr.* **25,** 306–328 (1995).
30. Osborn, T. R. Estimates of the local rate of vertical diffusion from dissipation measurements. *J. Phys. Oceanogr.* **10,** 83–89 (1980).

Acknowledgements

This work is supported by China National Natural Science Foundation (NSFC) Outstanding Young Investigator Project (40788002), National Key Basic Research Program (2007CB411800), and NSFC Creative Group Project (40921004). We thank the International Argo (Array for Real-time Geostrophic Oceanography) Observational Program for providing data through the open access (http://wo.jcommops.org/cgi-bin/WebObjects/Argo.woa/wa/ptfSearch). Finally, we thank E. Kunze for an insightful explanation about abyssal mixing inferred from lowered ADCP shear and CTD Strain profiles.

Author contributions

L.W. and Z.J. made equal contributions to the paper. L.W. contributed to the central idea and organized the writing of the paper. Z.J. performed the data analysis and contributed to writing of the paper. S.R. and M.V. offered guidance in analyses of the Argo profiling data and mixing, and contributed to the editing of this paper.

Additional information

The authors declare no competing financial interests. Reprints and permissions information is available online at http://www.nature.com/reprints. Correspondence and requests for materials should be addressed to L.W.